

BSAC-CoEx: Coexistence of URLLC and Distributed Learning Services via Device Selection

Milad Ganjalizadeh, Hossein S. Ghadikolaei, Deniz Gündüz, and Marina Petrova

Abstract—Recent advances in distributed intelligence have driven impressive progress across a diverse range of applications, from industrial automation to autonomous transportation. Nevertheless, deploying distributed learning services over wireless networks poses numerous challenges. These arise from inherent uncertainties in wireless environments (e.g., random channel fluctuations), limited resources (e.g., bandwidth and transmit power), and the presence of coexisting services on the network. In this paper, we investigate a mixed service scenario wherein high-priority ultra-reliable low latency communication (URLLC) and low-priority distributed learning services run concurrently over a network. Utilizing device selection, we aim to minimize the convergence time of distributed learning while simultaneously fulfilling the requirements of the URLLC service. We formulate this problem as a Markov decision process and address it via BSAC-CoEx, a framework based on the branching soft actor-critic (BSAC) algorithm that determines each device’s participation decision through distinct branches in the actor’s neural network. We evaluate our solution with a realistic simulator that is compliant with 3GPP standards for factory automation use cases. Our simulation results confirm that our solution can significantly decrease the training delays of the distributed learning service while keeping the URLLC availability above its required threshold and close to the scenario where URLLC solely consumes all wireless resources.

Index Terms—6G, URLLC, device selection, distributed learning, factory automation, reinforcement learning, soft actor-critic.

I. INTRODUCTION

THE envisioned 6G networks seek to go beyond mere connectivity by embedding intelligence into all aspects of communication. This evolution paves the way for a cyber-physical ecosystem that seamlessly connects devices, artificial intelligence (AI), and humans [1], [2]. In parallel, a growing wave of AI services has demonstrated remarkable performance gains across diverse use cases, from enhanced mobile broadband (eMBB) [3] to industrial control [4] and self-driving vehicles [5]. However, these gains hinge on large-scale model training, a process often hindered by data privacy concerns, limited wireless resources, and the widespread distribution of devices possessing data.

To mitigate these challenges, privacy-preserving distributed learning has emerged as a promising solution, allowing edge devices to train AI models collaboratively without sharing raw local data. Typically, multiple devices upload local updates (e.g., local models in federated learning (FL) [6] or local gradients in distributed gradient descent (DGD) [7]) using the uplink (UL) channel to a central node (or a set of nodes). The central node maintains the global parameters and orchestrates

each iteration of distributed training. Once it updates the global model, it transmits the new parameters to devices via the downlink (DL) channel, initiating the next iteration.

The wall-clock convergence time of a distributed learning algorithm depends on i) the number of required training iterations to reach a certain optimality gap, and ii) the delay of each training iteration (which includes the UL/DL transmission of local updates/global model parameters, and computation at devices and the central node). The former depends on various factors, such as the model size, data quality, selected learning algorithm and its hyperparameters [8], [9]. Under ideal processing and communication assumptions, increasing the number of participating devices at each iteration often leads to a better convergence rate, resulting in a shorter convergence time. However, when implemented across wireless devices, because of interference and limited available bandwidth, the training delay is impacted not only by the model parameters and the learning algorithm but also by the wireless channel resources between the central node and individual devices. In this case, while more participating devices may reduce the required number of iterations, it can extend the convergence time due to increased communication and computation delays [9].

Ultra-reliable low latency communications (URLLC) is characterized by its stringent requirements, demanding delays as short as $500\mu\text{s}$, and availability up to 99.999999 [10]. In [10], [11], 3rd Generation Partnership Project (3GPP) defines *communication service availability* as the mean proportion of time during which the communication service satisfies the required quality of service (QoS) of the application it serves. URLLC services are central to mission-critical industrial applications (such as robotics and factory automation) where even minor delays can lead to costly outcomes [12].

In this paper, we investigate optimizing the coexistence of URLLC and distributed learning services from communication perspective. This integration exemplifies the broader *AI-RAN* paradigm [13], which aims to enable AI services to share infrastructure with conventional services, utilizing additional communication and computation resources.

A. Motivations

There is a rich literature on conventional mixed services between URLLC and eMBB (e.g., [14]–[16]), URLLC and massive machine type communication (mMTC) (e.g., [17]), or even all three (e.g., [18]). However, the existing solutions may not be suitable to govern the coexistence of URLLC and distributed learning services for the following reasons:

- There are two fundamental differences between distributed learning and other conventional communication services. First, the performance of these conventional

services is characterized by the statistics of a communication metric (e.g., throughput for eMBB and energy consumption for mMTC). In contrast, distributed learning services are iterative and collaborative tasks aiming to solve an optimization problem. Besides, the potential statistical correlation of data from various devices enables distributed training to operate using only a subset of devices. Second, it has a unique set of decision variables such as the model size, choice of algorithm, and selection of devices participating in the training task.

- URLLC traffic affects the convergence time of distributed training in unique ways due to its higher traffic priority and strict requirements. For example, if URLLC devices have more intensive traffic or stricter availability requirements, low-priority services, including distributed learning, may face performance degradation due to fewer available physical resource blocks (PRBs). Alternatively, more participating devices in the training could increase the interference footprint and harm URLLC performance. A proper device selection strategy can alleviate such performance degradation. This is possible due to the unique properties of distributed learning applications and their robustness to occasional missing updates. The tighter the requirements of the coexisting service, the harder it is to design smooth coexistence.

Despite extensive research efforts to enhance the performance of URLLC and distributed learning over wireless networks as individual services, no studies to date have addressed the coexistence of these two services with both communication and learning aspects jointly considered. Nevertheless, numerous 6G applications leverage distributed learning to improve efficiency and system performance in areas such as industrial automation [4] and autonomous driving [5]. The successful adoption of these applications relies on analyzing and optimizing them alongside existing services, particularly URLLC, which poses the most demanding requirements. This serves as our primary motivation for this work.

B. Contributions

In this paper, we investigate an optimal coexistence of distributed learning and URLLC services. Our previous work [19] examined the mutual impact of these two services under 5G-NR protocols. Despite employing strict priority scheduling, we observed that the distributed training traffic could significantly influence the key performance indicators (KPIs) of URLLC and vice versa. In this work, we substantially extend [19] by expanding the system model, adding a new decision variable, developing new solution algorithms, and providing new engineering insights. In particular, we adopt a soft synchronous distributed learning protocol in which a central node broadcasts the global model updates upon receiving local updates from a subset of available devices. We then optimize the interplay between the two services. In summary, our contributions are as follows:

- We develop a model for the operational metrics of the URLLC service (i.e., communication service availability) and essential parameters that characterize distributed training workflow (i.e., training delay and convergence) and investigate the interplay between them. Since the system is resource-limited (in terms of bandwidth and transmission power) and URLLC requirements are strict, a subset of devices must be selected to perform each iteration of distributed training. Accordingly, we formulate an optimization problem that minimizes the average training latency to reach a given optimality gap while meeting URLLC's strict availability requirements.
- We transform the formulated coexistence optimization problem into a Markov decision process (MDP) and design an action masking technique to put a lower bound on the minimum number of devices required to participate in each iteration of distributed training. However, the solution may select a higher number of devices than this minimum to address the so-called *straggling effect*, where the lack of updates from some devices may halt the entire training.
- To deal with the unknown dynamics of our mobile network, we propose a data-driven approach that optimizes the device selection policy via a state-of-the-art off-policy deep reinforcement learning (DRL) algorithm, called BSAC-CoEx, a branching soft actor-critic (BSAC) framework designed for device selection in our coexistence scenario. In BSAC-CoEx, the selection policy of each device is distributed across distinct neurons, resulting in a linear increase in the BSAC output size with the number of devices.
- We evaluate our framework using a 3GPP-compliant 5G simulator in a factory automation use case. The results reveal that our solution not only preserves URLLC availability nearly on par with standalone URLLC service, but also reduces median training delays by more than 20%, compared to the slicing setting with service-specific resource partitions. Our results provide valuable insights into the ongoing standardization activities of distributed learning [20], [21].

The rest of this paper is organized as follows. We provide the necessary preliminaries on distributed learning in Section II and define our system model in Section III. The performance metrics and problem formulation are described in Section IV. Section V presents the proposed MDP modeling and BSAC-CoEx framework. We describe our simulation methodology in Section VI, and discuss the results in Section VII. Finally, Section VIII concludes the paper.

Notations: Normal font x or X , bold font \mathbf{x} , bold font \mathbf{X} , and uppercase calligraphic font \mathcal{X} denote scalars, vectors, matrices and sets, respectively. We denote by $[X]$ the set $\{1, 2, \dots, X\}$, by $[\mathbf{x}]_i$ element i of vector \mathbf{x} , by $[\mathbf{X}]_{i,j}$ the element ij of matrix \mathbf{X} , and by $|\mathcal{X}|$ the cardinality of set \mathcal{X} . We define $\mathbb{1}\{\mathbf{x}\}$ as the element-wise indicator function returning \mathbf{y} , where $[\mathbf{y}]_i$ takes 1 when condition $[\mathbf{x}]_i$ holds, and 0, otherwise. The curled inequality (\geq or $>$) represents element-wise inequality. We use $\mathbf{1}$ and $\mathbf{0}$ to denote all-one and all-zero vectors, respectively, and \mathbb{N} to denote the set of natural numbers. Table I summarizes our main notations.

II. DISTRIBUTED LEARNING OVER WIRELESS NETWORKS

We consider the problem of minimizing a sum of smooth functions $\{f_i : \mathbb{R}^d \mapsto \mathbb{R}\}_{i \in [N]}$, with corresponding gradients $\{\nabla f_i : \mathbb{R}^d \mapsto \mathbb{R}^d\}_{i \in [N]}$:

$$\mathbf{w}^* := \min_{\mathbf{w} \in \mathbb{R}^d} f(\mathbf{w}) = \min_{\mathbf{w} \in \mathbb{R}^d} \frac{1}{N} \sum_{i \in [N]} f_i(\mathbf{w}), \quad (1)$$

where f is the global loss function, each f_i represents a local loss function, and N is the number of distributed devices. In practice, we may use distributed algorithms to solve (1) to expedite the computations or to preserve the privacy of local datasets [22]. At the k th iteration, a subset of workers compute their local gradients and share them with a central node, which maintains the global model. The central node updates and broadcasts \mathbf{w}_{k+1} back to the workers.¹ FL is another method in which the workers share their updated local models instead of the gradients. Subsequently, the central node takes a global average over them. The communication overhead is almost the same as uploading gradients [24].

On the one hand, most of these UL messages (gradients or local models) may be redundant since they can be retrieved from past messages or messages from other devices [25]. On the other hand, the central node must wait for all the participating devices to send their updates, which results in considerable idle time for the central node and delays for faster devices waiting for stragglers to complete their updates. To tackle the straggling issue, in soft synchronous approaches, the central node only waits for a subset of participating devices, say n out of all N devices, to update the global model at each iteration [7]. Reference [26] proposed an algorithm to adjust n at each iteration. However, vanilla n -sync-based approaches increase the load on the underlying communication system by demanding all devices to upload their typically large model parameters and starting the update process at the central node only after receiving the first n messages. Forcing some of the devices to remain silent would i) reduce UL interference to other users, ii) improve latency, and iii) increase throughput. References [6], [25], [27] proposed various techniques to eliminate unnecessary uploads.

Running distributed learning over wireless networks presents additional challenges; not only due to the scarcity of resources (e.g., bandwidth and transmit power), but also because of the wireless propagation dynamics—affected by factors such as noise, interference, and fading [9]. To address these challenges, several recent studies have focused on resource management and, more explicitly, device selection techniques to improve the performance of distributed training in terms of training loss or convergence time [28]–[34]. For example, in [28], the authors evaluated the impact of resource management, device selection, and transmit power on FL convergence, and optimized these parameters to reduce FL training loss. Reference [29] proposed an FL algorithm that can handle heterogeneous user data assuming strong convex and smooth loss functions. The resource allocation

was then optimized to improve the convergence of the proposed algorithm. Unlike previous model-based approaches, references [30]–[33] utilized DRL to perform device selection. A device selection policy, jointly based on computation speed and channel condition, is proposed in [35]. Global model delivery to the devices over a noisy DL channel is studied in [36]. In [34], it is shown that distributed training performance can be improved if the device selection algorithm jointly considers the updates from the devices with their channel conditions. Reference [37] introduces a device selection and scheduling framework for the fair selection of edge devices in clustered federated multitask learning, ensuring fair participation opportunities during training. This approach enhances convergence speed and mitigates biases in the resulting global models. Nevertheless, none of these works address scenarios involving mixed services, where wireless network characteristics and limitations, along with demands on the higher-priority service, determine distributed learning performance.

III. SYSTEM MODEL

A. Network Model

In the context of industrial automation, which is one of major use cases of URLLC services [12], we consider a scenario where a set of $\mathcal{G} := [G]$ gNodeBs (gNBs), each consisting of one cell, serve a set of $\mathcal{U} := [U]$ URLLC devices, executing different functions that enable automated production. The communication system should timely and reliably deliver i) computed or emergency control commands to the actuators, and ii) monitoring data to gNBs. To simplify our analysis, we assume that the devices participating in the learning process are distinct from the URLLC devices, and for distinction, we will call the former AI devices. We consider a set of $\mathcal{N} := [N]$ AI devices, orchestrated by a single parameter server (i.e., central node) to carry out a single distributed learning task. We assume that the central node waits until receiving the local model update from n out of these N AI devices at each iteration. To tackle the straggler effect, the central node might request an update from $\mathcal{N}_{m,k} \subseteq \mathcal{N}$ of the AI devices at iteration k , where $|\mathcal{N}_{m,k}| = m_k (\geq n)$ (i.e., the central node might request $m_k - n$ extra backup devices to mitigate the straggler problem).

In the context of 5G and beyond, two approaches are proposed to manage the coexistence of two services with different priorities. The first approach is to leverage the existing standardized protocols in 5G-NR for QoS handling. The second approach involves creating separate slices for URLLC and distributed learning services, thus resulting in complete resource isolation. We employ the former approach. In this scenario, each connected device is assigned one or more QoS flows and data radio bearers. The QoS flows are determined based on the service's QoS requirements and configured in the core network. For instance, in our specific case, traffic from or to URLLC devices is given a high-priority QoS flow to ensure minimal latency. These QoS flows are then mapped to data radio bearers in the radio access network (RAN). Both the gNB and devices have an associated radio link control (RLC) buffer for each data radio bearer, with strict priority scheduling applied in our case, as described in [38].

¹We have a similar set of trade-offs and solutions for non-smooth functions, where we cannot define gradients. The major difference compared to this paper is that instead of updating based on gradients, we may need to update based on its generalizations, like subgradients [23].

B. Distributed Learning Process

We consider a network of N AI devices that cooperatively solve a distributed learning problem. Assuming that $\mathcal{N}_{n,k} \subseteq \mathcal{N}_{m,k}$ is a subset of size n , whose updates the central node receives first at iteration k , then iteration k of an abstract distributed algorithm reads:

$$\mathbf{w}_{k+1} = A(\mathbf{c}_{i,k}, \mathbf{w}_k), \quad \text{for } \forall i \in \mathcal{N}_{n,k}, \quad (2a)$$

$$\mathbf{c}_{i,k} = C_i(\mathbf{w}_k), \quad \text{for } \forall i \in \mathcal{N}_{m,k}, \quad (2b)$$

where function A represents an algorithm update of the decision variable \mathbf{w}_k , function C_i picks out the relevant information, $\mathbf{c}_{i,k}$, that device i uploads to the server for algorithm execution. This general algorithmic framework accommodates a variety of machine learning algorithms, including FL and DGD, with or without data compression. For instance, when C_i yields a stochastic gradient, say $\widehat{\nabla} f_i(\mathbf{w}_k)$, and $A = \mathbf{w}_k - \eta \sum_i \widehat{\nabla} f_i(\mathbf{w}_k)/n$ for some positive step size η , we obtain n -sync and synchronous DGD for $n(<N)$ and $n(=N)$, respectively [7]. When C_i returns the updated local model parameters of the i th AI device and A performs an averaging step over a subset of $n(\leq N)$ AI devices, we recover federated averaging [6] (either n -sync or synchronous).

C. Channel Model

To model the channel, we consider a multiple-input and multiple-output system in which we leverage the 3D spatial channel model from 3GPP in [39]. In this model, channels are characterized via clustering the multipath components, arriving at antenna arrays, in delay and double-directional angle (i.e., the zenith and azimuth of the angle-of-arrivals at the receiver and angle-of-departures at the transmitter). We have moved the details of the channel model to Appendix B. Notice that our problem formulation (Section IV-C) and solution approach (Section V) are general and not limited to this channel model.

For clarity and convenience, the symbols and notations used throughout this paper are summarized in Table I.

IV. PERFORMANCE METRICS AND PROBLEM FORMULATION

A. URLLC KPI: Communication Service Availability

The convergence of operational, information, and communication technologies through 5G is paving the way for connected industries. However, this integration poses a significant challenge of ensuring that the operational requirements are met during the 5G system's operating phase [40]. One well-accepted metric in the operational technology domain is *availability*. Hence, 3GPP, as the primary standardization consortium for mobile telecommunications, has attempted to specify the requirements for communication service availability from the application layer perspective in [10], [11]. The main difference between the network performance and the observed performance on the application layer is driven by a system parameter called *survival time*, T_{sv} . Survival time is the period of time for which the application layer can continue to function without receiving an expected packet [41]. We denote the network layer state by a Bernoulli random

TABLE I: Main Symbols and Notations

Symbol	Description
$\mathcal{N}, \mathcal{U}, \mathcal{G}$	Sets of AI devices, URLLC devices, and gNBs.
π_k^u, m_k	Device-selection vector at iteration k and the number of selected devices.
n	Minimum required number of local updates per iteration (n -sync), $m_k \geq n$.
d_k^{AI}	Distributed training delay in iteration k .
$\mathbf{w}_k, \mathbf{w}^*$	Global model at iteration k , and optimal global model.
K_{\min}, ϵ	Number of global iterations for convergence, and tolerance parameter defining ϵ -optimality.
α_i^Γ	URLLC device i 's availability in $\Gamma \in \{\text{UL}, \text{DL}\}$.
α_i^{req}	URLLC device i 's availability requirement.
γ	Tolerable violation probability in $\Pr\{\alpha_i^\Gamma \leq \alpha_i^{\text{req}}\} \leq \gamma$.
T_{sv}	Survival time for URLLC application-layer continuity.
$\mathbf{s}_k, \mathbf{a}_k, r_k$	State, action, and reward of iteration k , respectively.
λ, ψ	Discount factor and temperature parameter in SAC.
$\mathbf{H}_{x,y}(\tau; t)$	MIMO channel impulse response between device x and gNB y .
N_g, N_d	Number of gNB antennas and device antennas.
N_c, N_s	Number of clusters and rays in the spatial channel model.
$\beta^{x,y}$	Large-scale fading for device x to gNB y .
Pr_{LOS}	Probability a link is in LOS.
PL_{LOS}	Pathloss under LOS conditions.
PL_{NLOS}	Pathloss under NLOS condition.
$d_{x,y}^{2D}, d_{x,y}^{3D}$	2D and 3D distance between device x and gNB y .

variable $X_i^\Gamma(t)$, where $\Gamma \in \{\text{UL}, \text{DL}\}$, and $X_i^\Gamma(t)$ for the i th URLLC device is zero (i.e., link outage) if the last packet is not received at the communication interface within a specified delay bound, because either it could not be decoded at the lower layers or faced excessive retransmission and/or queuing delays. Assuming negligible application recovery time, we then define the per-device application layer state variable as

$$Y_i^\Gamma(t) := \begin{cases} 0, & \text{if } \int_{t-T_{sv}}^t X_i^\Gamma(\tau) d\tau = 0 \text{ (failure),} \\ 1, & \text{otherwise (operational).} \end{cases} \quad (3)$$

Thus, we can define the long-term communication service availability for the i th URLLC device in Γ direction as [42]

$$\alpha_i^\Gamma := \lim_{t \rightarrow \infty} \Pr\{Y_i^\Gamma(t)=1\} = \lim_{T \rightarrow \infty} \frac{1}{T} \int_0^T Y_i^\Gamma(t) dt. \quad (4)$$

The availability in Γ direction can be estimated over a short time period using

$$\hat{\alpha}_i^\Gamma(\Delta t_k) := \frac{1}{\Delta t_k} \int_{t_k}^{t_k + \Delta t_k} Y_i^\Gamma(t) dt. \quad (5)$$

In URLLC, the requirement is often defined in the form of [43]

$$\Pr\{\alpha_i^\Gamma \leq \alpha_i^{\text{req}}\} \leq \gamma, \quad \forall i \in \mathcal{U}, \quad (6)$$

where α_i^{req} is the communication service availability requirement of the use case that URLLC device i belongs to, and γ is the maximum tolerable violation probability, which is determined by the sensitivity of this use case to α_i^{req} . We follow [10] in assuming that the requirement for UL and DL availability is the same for a given use case.

B. Distributed Learning KPI: Convergence Time

The convergence time of distributed learning algorithms is bounded by the communication and processing latency [9].

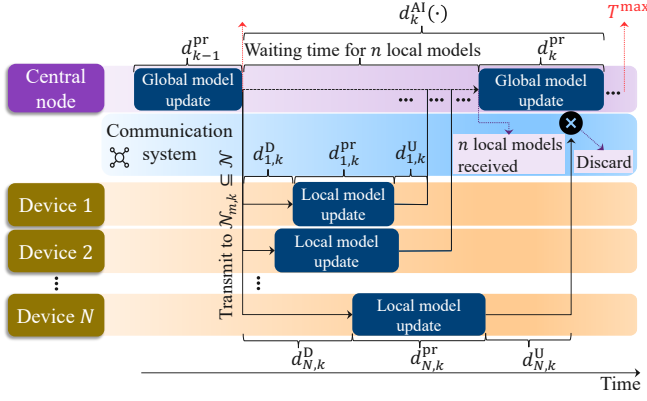


Fig. 1: The illustration of training delay in distributed AI workflow.

Let us denote the device selection at iteration k by an indicator vector $\pi_k^u = [\pi_k^u, \pi_k^u, \dots, \pi_k^u]$, where $[\pi_k^u]_i \in \{0, 1\}, \forall i \in \mathcal{N}$. Assuming that the central node requests the subset $\mathcal{N}_{m,k}$ (i.e., $\mathbf{1}^T \pi_k^u = m_k$) to participate in the training while it only waits for n local updates, the training delay at the central node for the k th iteration, d_k^{AI} , can be derived as

$$d_k^{\text{AI}}(\Pi_k^u) := \min \left\{ \min_{\substack{\mathcal{N}_{n,k} \subseteq \mathcal{N}_{m,k}, \\ |\mathcal{N}_{n,k}|=n}} \left(\max_{i \in \mathcal{N}_{n,k}} (d_{i,k}^D + d_{i,k}^{\text{pr}} + d_{i,k}^U) \right) + d_k^{\text{pr}}, T^{\max} \right\}, \quad (7)$$

where $\Pi_k^u := [\pi_k^u, \dots, \pi_k^u]$ is the device selection matrix, $d_{i,k}^D$, $d_{i,k}^{\text{pr}}$, and $d_{i,k}^U$ denote the latency associated with the transmission of the global model from the central node to user equipment, local training (as in (2b)), and transmission of local parameters from the user equipment to the central node for the k th iteration of device i , respectively. Note that both $d_{i,k}^D$ and $d_{i,k}^U$ encapsulate the transmission processing, payload transmission, occurred retransmissions, and queuing delay. Thus, both are inherently functions of Π_k^u . Additionally, d_k^{pr} represents the processing delay in executing (2a) on the central node for the k th iteration. Consequently, in (7), for each subset of $\mathcal{N}_{n,k}$ with a cardinality of n , the maximum aggregated communication and processing delay is calculated among devices. To determine $d_k^{\text{AI}}(\cdot)$ among these subsets, we select the subset with the lowest delay, subject to a maximum permissible delay of T^{\max} for every iteration. In Section V, we develop a computational method to calculate all these delay components. Fig. 1 illustrates the training delay in n -sync distributed training.

We denote by K_{\min} the iteration number after which the distributed learning algorithm converges. To characterize K_{\min} , we define ‘‘critical points’’ as the set of points where the norm of their derivative is 0. The local minima and maxima are a subset of these points [44]. Note that a critical point may not necessarily be an optimal point, e.g., a saddle point. To identify these critical points, we apply the first-order necessary condition by searching for the points at which the gradients vanish. In practice, for computational efficiency, we assume that the global model converges when the approximate first-order necessary condition is met, and terminate the algorithm

accordingly. Hence, we can formally define K_{\min} as

$$K_{\min} := \min \left\{ k \mid \mathbb{E} \left[\|\widehat{\nabla} f(\mathbf{w}_k)\|_2 \right] \leq \epsilon, k \in \mathbb{N} \right\}, \quad (8)$$

where ϵ is a small positive constant. The K_{\min} value varies depending on the specific problem setting and learning properties. We can use either numerical or theoretical approaches to determine K_{\min} . In our experiments, we rely on numerical approximations to obtain K_{\min} . Nevertheless, as demonstrated in Appendix A, we can also theoretically approximate K_{\min} for DGD and FL under smoothness, strong/non-convexity, and a few other technical assumptions related to the objective functions. Examples shown in Appendix A indicate that the value of K_{\min} decreases as the number of devices participating in the global update (i.e., n) increases.

C. Problem Formulation

Having defined the system model and performance metrics, the next step is to design a device selection scheme that optimizes the distributed training process by minimizing its convergence time while still meeting URLLC availability requirements.

Assuming an n -sync scheme and considering $d_k^{\text{AI}}(\Pi_k^u)$, K_{\min} , and the availability requirement in equations (7), (8), and (6), respectively, we formulate the following optimization problem:

$$\min_{\Pi_k^u} \sum_{k=1}^{K_{\min}} d_k^{\text{AI}}(\Pi_k^u), \quad (9)$$

$$\text{s.t. } \Pr \{ \alpha_i^\Gamma \leq \alpha_i^{\text{req}} \} \leq \gamma, \forall i \in \mathcal{U}, \forall \Gamma \in \{\text{UL}, \text{DL}\}, \quad (9a)$$

$$\mathbf{1}^T \pi_k^u \geq n, \forall k \in [K_{\min}], \quad (9b)$$

$$\pi_k^u \in \{0, 1\}^N, \forall k \in [K_{\min}]. \quad (9c)$$

where $\mathbf{1}^T \pi_k^u = m_k$ and $m_k \in [n, N], \forall k \in [K_{\min}]$. The objective of (9) is to minimize the convergence time, which is defined as the sum of the training delays until the distributed training process achieves ϵ -optimality. Constraint (9a) ensures URLLC service availability, as specified by (6). To fulfill the required number of local updates in the global update of (2) in the n -sync scheme, (9b) enforces the central node to select at least n AI devices and yet it is flexible in selecting any number of extra devices to tackle the straggling problem. Moreover, condition (9c) indicates that the device selection policy is a binary vector. Note that (9b), and (9c) must be respected at all decision time epochs.

On the one hand, the communication service availability of each URLLC device is a function of the channel state variable, $X_i^\Gamma(t)$, and the end-to-end delay of its packets. These two depend on many variables, such as instantaneous signal to noise and interference ratio (SINR), selected modulation and coding scheme (MCS), and transmission buffer status. On the other hand, these variables also impact the delay of the selected AI devices, influencing the training delay for each iteration. In addition, since the URLLC service has higher priority than the distributed learning service, the amount of URLLC traffic being served on the corresponding gNB severely affects the training delays.

The optimization problem (9) focuses exclusively on tuning the hyper-parameters for URLLC. However, the real-time operational aspects of URLLC (e.g., transmit power decisions, retransmissions, and PRB allocation) can be further refined through a nested control loop approach. In this framework, (9) serves as the outer control loop, while the real-time URLLC optimizations are handled by an inner control loop operating on a shorter timescale.

V. DEVICE SELECTION OPTIMIZATION

In optimization problem (9), characterizing the impact of device selection policy on our KPIs necessitates explicit modeling of the channel, queues and delay components of Equation (7), which involves approximations that may not be accurate in practical scenarios. Therefore, we propose to model the device selection problem as a finite horizon MDP.

In Section V-A, we specify the state space \mathcal{S} , action space \mathcal{A} , and all possible rewards, \mathcal{R} , based on dynamic interactions between the central node and RAN environment. Nevertheless, due to the complexity and dynamicity of our environment, deriving the transition probability function ($p : \mathcal{S} \times \mathcal{R} \times \mathcal{S} \times \mathcal{A} \mapsto [0, 1]$) is impractical. Therefore, in Section V-B, we apply a model-free DRL algorithm to solve this MDP problem. Our solution is based on BSAC [42], an extension of the celebrated soft actor-critic (SAC) algorithm [45]. BSAC addresses the large action space challenge we observe in the optimal coexistence of URLLC and distributed learning services.

A. Transformation to MDP Problem

The essential elements of the MDP are defined as follows.

1) *State Space, \mathcal{S}* : The state space characterizes the environment. We categorize the environment's state at iteration k (i.e., $s_k \in \mathcal{S}$), into three classes i) the observations from each URLLC device, ii) the observations from each AI device, and the observations from each gNB. In the following, we describe these three classes.

URLLC QoS variables: Communication service availability of each URLLC device, as the main URLLC KPI, is a function of packet error ratio, mean outage duration, and survival time [41]. Except for survival time which is static and use case specific, the state should include both (UL/DL) packet error ratio and (UL/DL) mean outage duration, estimated via empirical measurements within $\Delta t_{k-1} := t_k - t_{k-1}$.² In addition to these measures that explicitly affect the communication service availability, cell association, (UL/DL) buffer size (at t_k), (UL/DL) SINR, and (UL/DL) delay are other metrics that implicitly impact the availability. However, SINR and delay statistics might vary significantly during, possibly long, Δt_{k-1} . Hence, we represent their distribution using specific statistics of these measures, i.e., 1st percentile, 5th percentile and median of the SINR distribution, and 95th percentile,

99th percentile, and median of the delay distribution. In fact, utilizing such percentiles is well motivated by URLLC extreme availability performance, which, under proper system design, is affected by the tail of delay and SINR distributions [46].

Distributed training delay variables: The training delay of each iteration, $d_k^{\text{AI}}(\Pi_k^u)$, is a function of the device selection; thus, we include a binary variable in the state indicating if this device has been selected in the last iteration. As indicated by (7), the delay of the DL transmission of the global model, $d_{i,k}^{\text{D}}$, and the delay of the UL transmission of local parameters, $d_{i,k}^{\text{U}}$, directly impact the training delay, and thus, should be included in the state. Besides, (UL/DL) buffer size (at t_k), and (UL/DL) SINR of the underlying transmissions have an implicit effect on the delay, and therefore, we include them in the state as well. Focusing on the overall statistics (unlike URLLC service), we represent the SINR distribution of the underlying transmissions for each AI device with its 5th percentile, median and 95th percentile. Note that no empirical measurement exists for $d_{i,k}^{\text{D}}$, $d_{i,k}^{\text{U}}$, and SINR of AI devices whose central node does not receive their local models in the k th iteration (i.e., $i \notin \mathcal{N}_{n,k}$). Moreover, if an AI device was selected at t_{k-1} , but its local update is not among the first n received, its buffer size at t_k would not be empty.

gNB level observations: At the gNB level, the consumption of PRBs by each service (both in UL and DL directions) has a significant impact on training delay and availability. To address this, we propose adding the mean number of allocated PRBs per slot within Δt_{k-1} for each service to the state.

2) *Action Space, \mathcal{A}* : The action space is the set of all possible decision variables enabling the DRL agent to interact with its environment. Considering (9), our action vector at the k th iteration should be the device selection vector π_k^u , and thus $|\mathcal{A}| = 2^N$.

3) *The Reward Function, r* : In general, the DRL agent follows an explicit goal, i.e., to maximize its cumulative discounted rewards. In other words, the reward function, r_{k+1} , is the payoff for taking action a_k at state s_k . As (4) indicates, the communication service availability of URLLC devices is measured in infinite time, whereas the temporal granularity of the DRL is determined by the amount of time each distributed training round takes, Δt_k . Therefore, we suggest using the availability estimator from Equation (5) as part of the reward function. While estimating such long-term measures over a short step period might introduce inaccuracies, this estimation does represent the immediate influence of the device selection policy on the application layer performance [42]. A conventional approach to address constraints of (9) uses a regularized reward function, where a penalty term is incorporated to penalize constraint violations [47], [48]. Accordingly the reward for iteration k , r_{k+1} , is defined as

$$r_{k+1} := \nu \exp \left(\zeta \min \left\{ \min_{i \in \mathcal{U}, \Gamma \in \{\text{UL}, \text{DL}\}} \left(\hat{\alpha}_i^\Gamma(\Delta t_k) - \alpha_i^{\text{req}} \right), 0 \right\} \right) + (1 - \nu) \frac{T_{\text{max}} - d_k^{\text{AI}}(\Pi_k^u)}{T_{\text{max}}}, \quad (10)$$

²Notice that our two services operate on different time scales: URLLC performance should be evaluated based on the actual time, whereas the control loop's time step is defined as one iteration of the distributed learning algorithm (i.e., $d_k^{\text{AI}}(\cdot)$ for the k th iteration). Hence, the control loop is not periodic in actual time and is triggered by the central node. Accordingly, we use $\Delta t_k = t_{k+1} - t_k$ to emphasize the time instants when iteration k begins and ends.

where $v(\in [0, 1])$ is the weight characterizing the relative importance between the URLLC and distributed learning rewards. In the URLLC reward, $(\hat{\alpha}_i^\Gamma(\Delta t_k) - \alpha_i^{\text{req}})$ is negative for those URLLC devices that did not meet their corresponding availability requirement within Δt_k , regardless of the transmission direction, Γ . Hence, our reward function enforces the DRL agent to maximize the availability of the worst URLLC device among those that do not meet their availability requirements. In addition, ζ is a design parameter, which is a function of the sensitivity (γ), and the precision that the maximum availability requirement needs (i.e., ζ is proportional to $\max_i(\alpha_i^{\text{req}})/\gamma$). Nevertheless, the device selection policy gets the full reward on the URLLC part (i.e., v) when all of the devices fulfill their availability requirements. For the distributed learning reward, the shorter $d_k^{\text{AI}}(\cdot)$ is, the larger the π_k^u 's reward becomes. Moreover, to minimize the tail of the per-device availability distribution and the average training delay, URLLC reward decreases exponentially while the reduction in distributed learning reward is linear.

B. Solution With BSAC-CoEx Framework

The BSAC-CoEx framework extends the SAC algorithm [45], integrating two additional features. First, drawing on insights from our previous work [42], we model the participation decision for each device using separate neurons in the last layer of the actor's deep neural network (DNN), resulting in considerable scalability gains. Second, we employ a simple action masking technique to ensure that (9b) is fulfilled in all decision time epochs. Additionally, our framework enjoys the advantages of the original SAC algorithm: i) SAC is an off-policy model-free DRL algorithm in which explorations aim to identify an optimal policy that maximizes not only the expected accumulated discounted reward but also the expected entropy at each visited state, thus improving the stability and exploration [45], ii) SAC has an actor-critic architecture where the critic approximates state-action pair values, and the actor determines the policy, and iii) SAC conquers the massive sampling complications and minimizes the sensitivity to its hyperparameters. In the rest of this section, we first introduce SAC for our problem, followed by a detailed description of BSAC-CoEx as implemented for our device selection problem.

The main objective in SAC is to find an optimal stochastic policy that maximizes the discounted sum of reward and entropy. Thus, the objective of SAC is

$$\pi^*(\cdot|\cdot) := \underset{\pi(\cdot|\cdot)}{\operatorname{argmax}} \sum_{k=1}^{K_{\min}} \mathbb{E} \left[\sum_{\kappa=k}^{K_{\min}-1} \lambda^{\kappa-k} \mathbb{E}[r_{\kappa+1} + \psi \mathbb{H}(\pi(\cdot|s_\kappa))] \right], \quad (11)$$

where $\lambda(\in [0, 1])$ and $\psi(> 0)$ are the discount factor and the temperature parameter specifying the relative importance between the reward and entropy terms, respectively [45]. Furthermore, $\mathbb{H}(\pi(\cdot|s_k)) := \mathbb{E}[-\ln(\pi(a|s_k))]$ is the entropy of policy π at state s_k . Introducing entropy in (11) guides the policy to explore more broadly while avoiding blatantly unfavorable trajectories.

The SAC algorithm (and actor-critic methods in general) uses policy iteration, in which the algorithm alternates between

policy evaluation (to compute the state-action value function by $Q_\pi(s, a)$) and policy improvement (to compute π) in the direction of maximizing the sum of discounted return (i.e., sum of reward and a portion of entropy here). In the policy evaluation step, using the soft Bellman backup equations, the soft state-action value function can be computed iteratively as follows [45]:

$$Q_\pi(s_k, a_k) = r_{k+1} + \lambda \mathbb{E}[Q(s_{k+1}, a_{k+1}) + \psi \mathbb{H}(\pi(\cdot|s_k))]. \quad (12)$$

In large-scale reinforcement learning problems where the state and action spaces are large, Q_π and π are approximated in each iteration using DNNs (via critics and actors, respectively). In BSAC-CoEx, we leverage target networks and clipped double Q-learning. Hence, in our architecture, there are 4 DNNs for the first critic, its target critic, the second critic, and its target, whose weights are denoted by $\varphi_1, \tilde{\varphi}_1, \varphi_2$, and $\tilde{\varphi}_2$, respectively. In addition, there are 2 DNNs for the actor and its target network, whose weights are denoted by ϑ and $\tilde{\vartheta}$, respectively. Thus, Q_π , in (12), is approximated by 2 DNNs as $Q_{\varphi_i}, i \in \{1, 2\}$. While SAC can handle both discrete and continuous actions, accommodating our action space with discrete actions requires the last layer of the actor networks to have as many neurons as the size of the action space, which leads to impractical memory and computational time requirements [42]. An alternative is to employ a single continuous action that is subsequently quantized to a discrete value, denoting the device participation for all AI devices. Nevertheless, due to a large action space and, thus, an enormous set of quantized values, the performance remains unsatisfactory. To overcome these limitations, in BSAC-CoEx, we represent a_k as a continuous vector. As discussed in Section V-A2, our action space \mathcal{A} has N dimensions for our device selection problem. Thus, each element $[a_k]_i \in \mathcal{A}_i, \forall i \in N$ indicates the action for the i th AI device, with \mathcal{A}_i denoting the action space of the i th dimension, which corresponds to the action space of the i th AI device. To eliminate discrete binary actions, we represent \mathcal{A}_i as continuous, and for sampling reasons described later, all elements are confined within tanh bounds (i.e., $[a_k]_i \in [-1, 1], \forall i \in N$). With this approach, the size of the actor networks' final layer increases linearly with the number of AI devices, avoiding the exponential growth associated with a discrete action space. Moreover, to mask out selections that do not follow condition (9b), we determine the mapping from a_k to π_k^u by

$$\pi_k^u := \begin{cases} \mathbb{1}\{a_k \geq \mathbf{0}\}, & \text{if } \mathbf{1}^\top \mathbb{1}\{a_k \geq \mathbf{0}\} \geq n, \\ \mathbb{1}\{a_k \geq a_k^{(n)} \mathbf{1}\}, & \text{otherwise,} \end{cases} \quad (13)$$

where $a_k^{(n)}$ is the n th largest element in vector a_k .

Let us assume the transitions are stored in a replay buffer, \mathcal{B} . Then, regardless of sampling technique (e.g., uniform or prioritized experience replay) and the mini-batch size ($|\mathcal{B}_{\text{mb}}|$), a sampled transition can be represented with (s, a, r, \hat{s}, I) , where I is a binary parameter that is 0 if the distributed learning converges in \hat{s} , and is 1, otherwise. Then, φ_1 and φ_2 can be trained by minimizing the mean squared error for

each sampled transition as

$$J_Q(\varphi_i) := \mathbb{E} \left[\frac{1}{2} \left(Q_{\varphi_i}(s, a) - \tilde{Q}(\hat{s}, \tilde{a}, r, I) \right)^2 \right], \quad (14)$$

where \tilde{a} is sampled from $\pi_{\tilde{\theta}}(\cdot | s_{k+1})$, and

$$\tilde{Q}(s, a, r, I) := r + I\lambda \left(\min_{i=1,2} Q_{\tilde{\varphi}_i}(s, a) - \psi \ln(\pi(a|s)) \right). \quad (15)$$

Note that the minimum represents the smallest Q-value between the two state-action value function approximations for clipped double Q-learning [49]. Then, in order to minimize $J_Q(\cdot)$, φ_1 and φ_2 are updated in the direction of gradient descent. To ensure that temporal-difference error remains low, we update target critics' weights gradually by $\tilde{\varphi}_i = \nu\varphi_i + (1-\nu)\tilde{\varphi}_i$ for $i \in \{1, 2\}$ at each DRL iteration.

In the policy improvement step, the actor DNN can be updated by minimizing the expected Kullback-Leibler divergence between π_{θ} and the exponential of the soft state-action value function, which can be rewritten as

$$J_{\pi}(\theta) := \mathbb{E} \left[\psi \ln(\pi_{\theta}(a|s)) - \min_{i=1,2} Q_{\varphi_i}(s, a) \right]. \quad (16)$$

To minimize $J_{\pi}(\cdot)$ based on the latest policy, we employ the re-parameterization technique, from [45], to reformulate the expectation over actions into an expectation over noise, leading to a smaller variance estimator. Therefore, we draw samples from an invertible tanh function of Gaussian policy such that $\tilde{a} := \tanh(\mu_{G,\theta}(s) + \sigma_{G,\theta}(s) \cdot \chi)$, where $\mu_{G,\theta}(\cdot)$ and $\sigma_{G,\theta}(\cdot)$ are the estimated mean and standard deviation of a Gaussian distribution, respectively, and χ follows a multivariate Gaussian distribution, with a mean of $\mathbf{0}$, and an identity matrix as its covariance matrix. Accordingly, we can reformulate $J_{\pi}(\theta)$ by replacing a with \tilde{a} in (16). The policy parameters, θ , are then updated in the gradient descent direction as in [45]. Additionally, we update the target actor weights smoothly by $\tilde{\theta} = \nu\theta + (1-\nu)\tilde{\theta}$.

Algorithm 1 summarizes the learning procedure of BSAC-CoEx. Leveraging the off-policy learning capability of such a framework, one can train the DNNs via either the virtual network (e.g., digital twin or realistic simulations) or an operating network (e.g., in safe exploration mode). On the former, a_k can be sampled using the behavior policy in each episode, and episodes can run in parallel to speed up the training. Nevertheless, on the operating network, this algorithm can switch to on-policy learning (i.e., a_k is sampled via the most updated policy, and episodes run consecutively). A hybrid strategy in which the DNNs are trained first with a virtual network and then tuned via an operational network could potentially result in a more efficient learning procedure.

Algorithm 1 was initially developed for single-task learning within a star topology, where computation occurs on a single server. However, minor modifications can alleviate both assumptions. First, in a multi-task learning scenario, the communication load among AI devices may increase without affecting the overall communication architecture and the skeleton of Algorithm 1. Nevertheless, it is necessary to adjust the definitions of parameters involved in the optimization problem (9). For instance, when training one independent model per

Algorithm 1: BSAC-CoEx Algorithm

Input: Set of AI devices \mathcal{N} , Required number of local models in global update n ;
Output: Device selection policy as a function of RAN state;
Initialize: φ_1 , φ_2 , and θ and set $\tilde{\varphi}_1 \leftarrow \varphi_1$, $\tilde{\varphi}_2 \leftarrow \varphi_2$, and $\tilde{\theta} \leftarrow \theta$, $k \leftarrow 1$;
episode: numbers of iterations during which distributed learning converges
foreach *episode* **do**
 Set initial device selection, from previous virtual training or random;
 while *true* **do**
 Receive $c_{i,k}$ from n AI devices, or T^{\max} ;
 Observe s_k (measured within Δt_{k-1});
 if $d_k^{\text{AI}} < T^{\max}$ **then** Compute w_{k+1} as in (2a);
 else $w_{k+1} \leftarrow w_k$;
 Sample an action, $a_k \sim \pi_{\theta}(\cdot | s_k)$;
 Transmit w_{k+1} , via RAN, to selected AI devices (π_k^u , derived from (13));
 Observe s_{k+1} , and calculate r_{k+1} via (10);
 if *distributed learning converges as in (8)* **then** $I_{k+1} \leftarrow 0$;
 else $I_{k+1} \leftarrow 1$;
 Store $(s_k, a_k, r_{k+1}, s_{k+1}, I_{k+1})$ in \mathcal{B} ;
 if $I_{k+1} = 0$ **then** break;
 $k \leftarrow k + 1$;
 end
 ▷ Training DNNs
 if $|\mathcal{B}| \geq |\mathcal{B}|_{\min}$ & $k = l|\mathcal{B}_{\text{mb}}|$, $\forall l \in \{1, 2, \dots\}$ **then**
 Randomly sample a mini-batch \mathcal{B}_{mb} from \mathcal{B} ;
 forall $(s, a, r, \hat{s}, I) \in \mathcal{B}_{\text{mb}}$ **do**
 Derive \tilde{Q} using (15), where $\tilde{a} \sim \pi_{\tilde{\theta}}(\cdot | \hat{s})$;
 end
 $\varphi_i \leftarrow \varphi_i - \frac{1}{|\mathcal{B}_{\text{mb}}|} \sum_{\forall b \in \mathcal{B}_{\text{mb}}} \nabla J_Q(\varphi_i)$, for $i \in \{1, 2\}$;
 $\theta \leftarrow \theta - \frac{1}{|\mathcal{B}_{\text{mb}}|} \sum_{\forall b \in \mathcal{B}_{\text{mb}}} \nabla J_{\pi}(\theta)$, where (16) uses \tilde{a} ;
 $\tilde{\varphi}_i \leftarrow \nu\varphi_i + (1-\nu)\tilde{\varphi}_i$ for $i \in \{1, 2\}$;
 $\tilde{\theta} \leftarrow \nu\theta + (1-\nu)\tilde{\theta}$;
 end
end

task, K_{\min} in (9) should be set to the maximum K_{\min} value across all individual tasks. Additionally, $d_k^{\text{AI}}(\cdot)$ should take into account the increased delay caused by communicating multiple models per iteration. Second, for other computation topologies (e.g., from a single parameter server to a multi-parameter server scenario to multi-tier tree topology), we need to account for extra communication overhead for parameter exchange among parameter servers. Again, notation-wise, (9) and Algorithm 1 remain unchanged, but we need to adjust the definitions of parameters characterizing K_{\min} and $d_k^{\text{AI}}(\cdot)$.

In the following section, we describe our simulator's modeling principles and its configuration.

VI. SIMULATION METHODOLOGY AND CONFIGURATION

For simulating the deployment where URLLC and distributed learning services coexist, we considered a factory automation scenario, which is one of the main use cases of URLLC services [12] (demonstrated in Fig. 2). More explicitly, we designed a 3D model of a small factory of size $40 \times 40 \times 10 \text{ m}^3$ with 4 gNBs at the height of 8 m, and with an inter-site distance of 20 m.

A. InF-DH Scenario

In our simulations, we employed the base 3GPP channel model of Appendix B for the indoor factory with dense clutter

VII. RESULTS AND DISCUSSION

For the performance evaluation, we set up two benchmarks.

- 1) Semi-random URLLC devices: In this benchmark, we set up 10 URLLC devices that move in a 1D space at a speed of 30 km/h, while remaining in close proximity to a fixed position that is maintained in different simulations. Yet, the movement direction of each device is randomly changed in different seeds.
- 2) Random URLLC devices: In this benchmark, we set up 20 URLLC devices. At each simulation, the URLLC devices appear at random positions and move in 1D in a random direction at a speed of 30 km/h within a short distance of that position.

The results of the first benchmark highlight how channel conditions and interference affect device selection, while those of the second benchmark provide insights into long-term system-level performance. For each of these benchmarks, we compared our solution (shown as BSAC-Coex in figures) against the following baselines:

- *singleURLLC*: We did not have any AI device in the factory, and the URLLC devices could consume the entire 40 MHz bandwidth and 0.5 W DL transmit power.
- *mix-RandSel(m)*: It involved both URLLC and AI devices sharing the wireless resources. We randomly selected a set of m participating devices (i.e., $m_k=m, \forall k \in \mathbb{N}$), where $m \in \{15, 20, 30, 40, 50\}$.
- *slic-RandSel(m)*: We dedicated 25% of resources to the URLLC service (i.e., 10 MHz bandwidth and 0.125 W for total DL transmit power), and the rest to the distributed learning service.³ Besides, we randomly picked a set of m participating devices (i.e., $m_k=m, \forall k \in \mathbb{N}$), where $m \in \{15, 20\}$.
- *mix-baseline*: This baseline is inspired by references [30]–[32] which minimize the convergence delay of federated learning via device selection, unaware of the potential coexisting services. As in *mix-RandSel(m)*, the wireless resources are shared in this baseline too. Device selection was executed using BSAC,⁴ ignoring the URLLC service representation. Thus, in this baseline, the state only contained distributed training delay variables and its PRB usage, and the reward in (10) was confined to the distributed learning part.
- *slic-baseline*: We sliced the bandwidth and transmit power as in *slic-RandSel(m)*. However, the device selection was performed as in *mix-baseline*.

The *singleURLLC* baseline represents the best possible performance on the URLLC availability in our scenario. For those baselines involving distributed learning service, we set $N=50$ and $n=15$ in BSAC-Coex, and to calculate the reward in (10), we set ν and ζ to 0.5, and 100, respectively. Besides, we assumed that all URLLC devices serve a single use

³In our experiment setup, we observed that allocating less than 25% of resources to URLLC traffic substantially increases the violation probability (formulated in (6)), making them unsuitable for the factory automation use cases.

⁴We had to replace the DRL solution algorithm with BSAC for memory and computation purposes. Convergence and scalability results of BSAC are out of the scope of this paper. Interested readers are referred to [42].

case, and thus, set the availability requirement to 0.99 (i.e., $\alpha_i^{\text{req}} = \alpha^{\text{req}} = 0.99, \forall i \in \mathcal{U}$). For *singleURLLC* evaluations, we conducted 102-second simulations 300 times with different seeds. The rest of the baselines were evaluated with at least 300 simulations of 50 iterations each, resulting in different simulation lengths. Note that there is no progress in distributed training if all n local models are not collected by the central node within a duration of T^{max} , and thus, DRL iterations may vary from distributed training iterations. Regardless, if there is no strict latency constraint from the distributed learning task, we can tune T^{max} sufficiently large to ensure that time-outs rarely happen. In our evaluations, we set $T^{\text{max}}=10$ s.

A. Semi-random URLLC Devices

Fig. 3 shows the distribution of our main KPIs. Fig. 3a illustrates the empirical cumulative distribution function (CDF) of URLLC devices' availability, where each sample is the UL or DL availability of one URLLC device in one simulation during its whole simulation time. The shaded area around each plot represents the 99.99% pointwise confidence bounds, determined using Greenwood's formula [53]. Fig. 3b depicts the training delay. Each box presents the minimum, 25th percentile, median, 75th percentile, and maximum values observed among the training delay samples. Together, these two figures present the coexistence performance.

In Fig. 3a, the availability distribution is identical for any arbitrary m in *slic-RandSel(m)* because of the dedicated resource slices for each service. As this figure shows, compared to *singleURLLC* and *slic-RandSel(m)*, the availability of the URLLC devices decreases in *mix-RandSel(m)*, $\forall m \in \{15, 20, 40\}$, likely because of the introduced interference by AI devices in the neighboring cells. Although the scheduler adjusts the MCS to deal with this additional interference,⁵ intensive distributed training traffic still affects the availability. Consequently, the 0.99 requirement is met with a violation probability of around 0.1, compared to roughly 0.01 in *singleURLLC*, *slic-RandSel(m)*, and BSAC-Coex, see Equation (6). In *mix-RandSel(m)* baselines, most of the availability samples remain above or equal to 0.98. However, unlike many conventional services, such a decrease is unacceptable for URLLC service. Despite the impact of introducing the large load of the distributed learning service, we observe that our BSAC-Coex solution keeps the URLLC devices' availability close to the *singleURLLC* and *slic-RandSel(m)* up to α^{req} . When it comes to training delay performance, as *slic-RandSel(m)* and *mix-RandSel(m)* boxes in Fig. 3b and our results in [19] suggest, training delay increases with the number of selected devices (i.e., as m grows). However, when $m=n$, it is more likely for the central node to wait excessively for stragglers and thus reach time-out (as in *slic-RandSel(15)* and *mix-RandSel(15)*). Moreover, the lower training delay statistics in *mix-RandSel(15)* and *mix-RandSel(20)*

⁵Note that such a decrease in availability occurs regardless of the scheduler configuration. For example, a higher target block error rate cannot overcome the extra interference, and a lower target block error rate leads to extra delay, both resulting in lower availability.

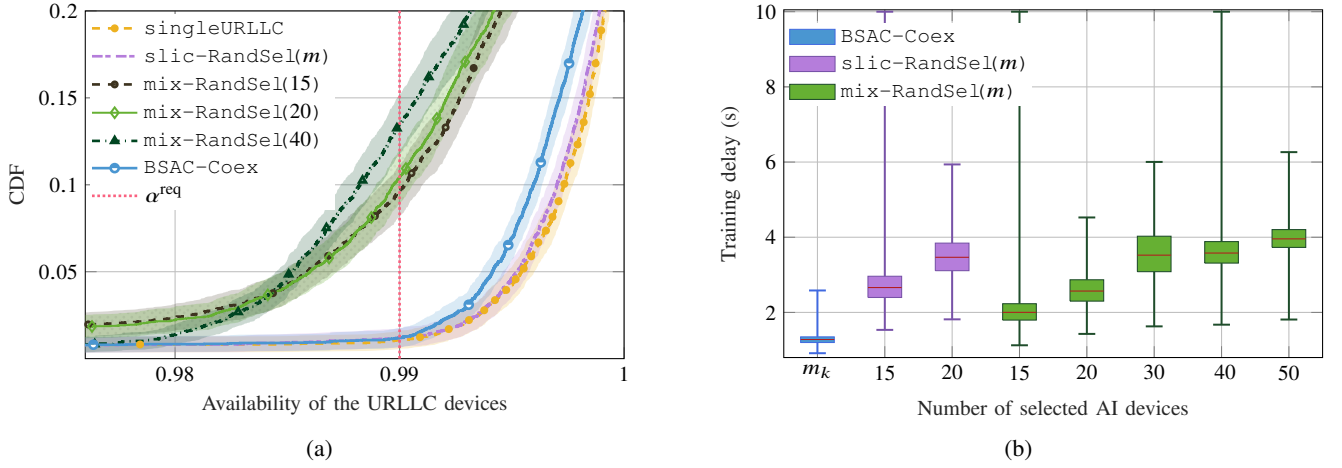


Fig. 3: Coexistence performance for the benchmark with semi-random URLLC devices. (a) Empirical CDF of URLLC devices' availability, $\hat{\alpha}_i^\Gamma$, where the shaded area around each plot indicates 99.99% confidence bounds. (b) Training delay, d_k^{AI} , where each box plot represents the minimum, 25th percentile, median, 75th percentile, and maximum of the training delay distribution.

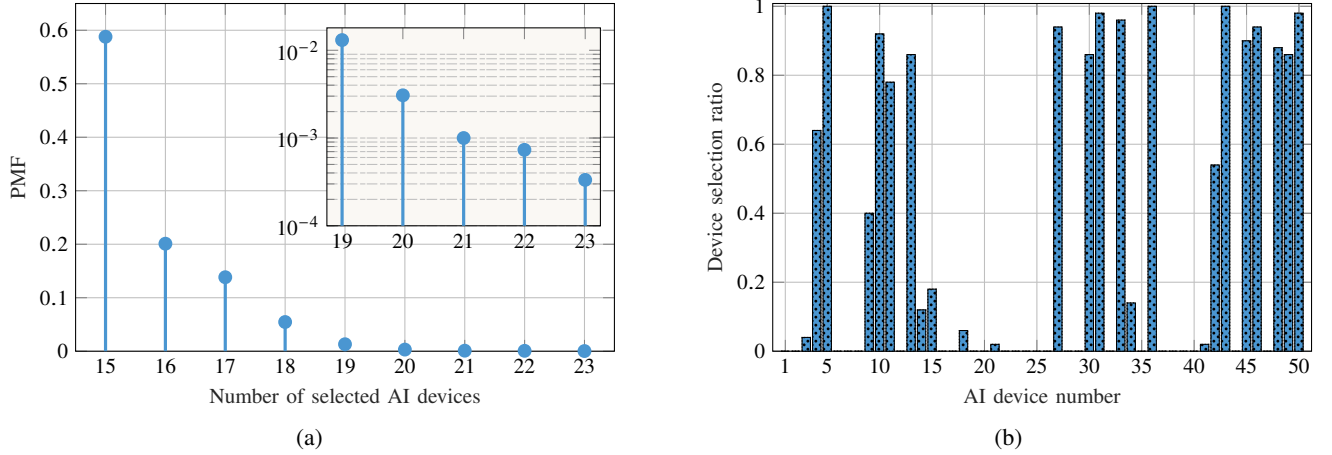


Fig. 4: Device selection policy of BSAC-Coex for the benchmark with semi-random URLLC devices. (a) Empirical PMF of the number of selected devices, m_k . (b) Participation ratio of each device.

than slic-RandSel(15) and slic-RandSel(20), respectively, suggests that distributed learning service in mix-RandSel(m) generally consumes more resources than the allocated resources in slic-RandSel(m). As this figure indicates, compared to the most competitive baseline (i.e., mix-RandSel(15)), our BSAC-Coex decreases the median training delay by 36%, while the maximum observed training delay is 2.6s, which is 43% less than that of mix-RandSel(20)—the baseline with the lowest maximum observed training delay. When URLLC traffic is well distributed and low per cell (as in this benchmark), BSAC-Coex can easily satisfy the URLLC requirements, as baselines like slic-RandSel(m). Yet, thanks to BSAC-Coex, the low-priority service experiences a much better training delay than those baselines, as shown in Fig. 3b. When URLLC traffic is high, meeting its requirements becomes more challenging for the baselines, but as we demonstrate in the next experiments, BSAC-Coex still succeeds in managing the coexistence.

Fig. 4 demonstrates the BSAC-Coex's device selection policy in the evaluation phase, π_k^u . Fig. 4a shows the empirical probability mass function (PMF) of the number of selected AI

devices, m_k . As this figure indicates, BSAC-Coex selected at least 1 extra backup AI device (i.e., $m_k - n \geq 1$) for more than 40% of iterations. Such selection of extra backup devices implies that our device selection solution could still leverage the diversity introduced by extra backup AI devices, even in our bandwidth-limited scenario. Carefully selected backup devices reduce the sensitivity to the straggler problem and, therefore, reduce the overall latency without substantially impacting the interference footprint. Fig. 4b represents the participation ratio of each AI device. As it shows, 9 AI devices are selected in over 90% of the iterations. Furthermore, 24% of the AI devices have a selection ratio ranging between 0.1 and 0.9, depending on their channel conditions, the loads of their corresponding cells, and the deployment specifics. In extreme cases, some of the devices may always (or never) be selected to participate in the distributed training.

B. Random URLLC Devices

Fig. 5 illustrates the empirical CDF of availability for URLLC devices (in Fig. 5a) and training delay of distributed

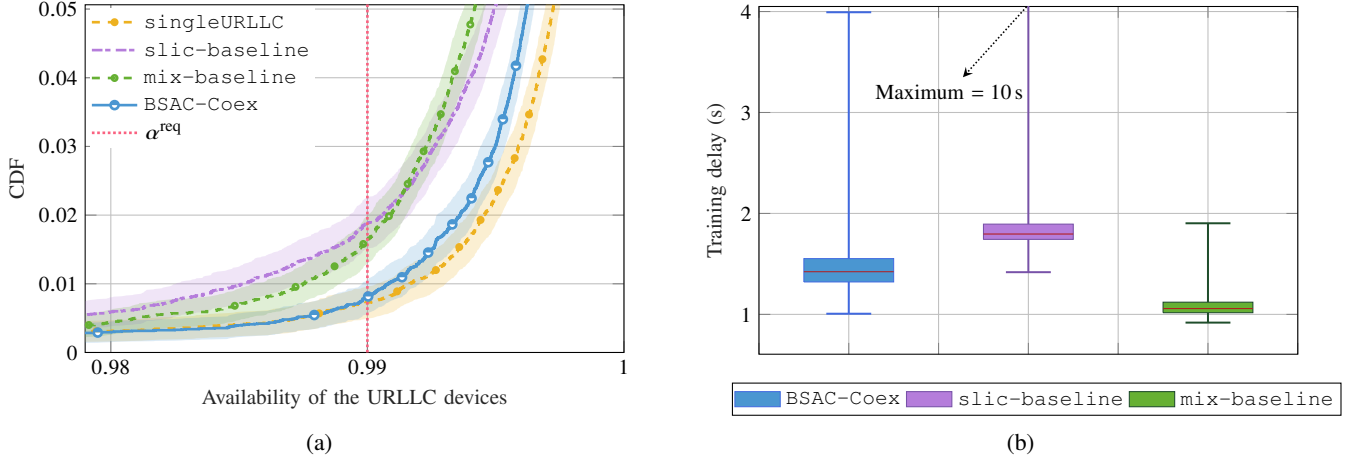


Fig. 5: Coexistence performance for the benchmark with random URLLC devices. (a) Empirical CDF of URLLC devices' availability, $\hat{\alpha}_i^F$, where the shaded area around each plot indicates 99.99% confidence bounds. (b) Training delay, d_k^{AI} , where each box plot represents the minimum, 25th percentile, median, 75th percentile, and maximum of the training delay distribution.

learning service (in Fig. 5b). As Fig. 5a shows, up to α^{req} , BSAC-Coex keeps the availability of URLLC devices close to singleURLLC (by only 0.0007 increase in γ), even though the URLLC traffic appears at random locations in different seeds. Surprisingly, slic-baseline meets a 0.99 availability requirement at a violation probability of $\gamma=0.019$, which is around 2.5x greater than singleURLLC and BSAC-Coex, and even 14% more than mix-baseline. It is worth noting that the availability distributions for slic-baseline and slic-RandSel(m) are identical due to the consistent operation of the URLLC slice in both baselines. In this benchmark, with twice the URLLC devices than the semi-random benchmark, many devices may be associated with the same gNB. Thus, in slic-baseline, the dedicated slice may be insufficient for certain gNBs across different seeds, leading to lower availability performance than baselines in which services share wireless resources. Nevertheless, as Fig. 5b shows, slic-baseline reaches higher training delays than other baselines too (with the median of 1.8 s and even occasional time-outs), indicating that the static slicing might cause resource deprivation for both services. However, Since mix-baseline only considers the distributed learning service performance, its γ to support α^{req} is 2.24x and 2.05x the violation probabilities of singleURLLC and BSAC-Coex, respectively. In Fig. 5b, BSAC-Coex achieves 1.42s median training delay, which is 34% higher than mix-baseline. This suggests that BSAC-Coex compensates an additional 360ms on the median training delay of the low-priority service to halve the violation probability of URLLC service's availability requirement.

VIII. CONCLUSIONS

In this paper, we investigated the performance optimization of distributed learning services coexisting with URLLC services. We proposed BSAC-CoEx, a novel framework that utilizes a carefully selected subset of devices for distributed training, aiming to minimize the convergence time of distributed learning while maintaining URLLC's stringent availability re-

quirements. Our comprehensive 3GPP-compliant simulations indicate that our scheme can significantly reduce the total training delay while maintaining the availability of URLLC devices close to that in the single service scenario (i.e., when URLLC devices exclusively utilize all network resources). Our results provide valuable insights into adaptively controlling distributed training traffic through device selection, ensuring sustainable coexistence between these two services.

An alternative approach to controlling the distributed training load is through the quantization of exchanged messages, thereby reducing the communication overhead per iteration and, consequently, the interference footprint. However, this reduction comes at the expense of requiring additional iterations to reach convergence. Potential future work includes developing novel methods that dynamically adjust the quantization level based not only on the distributed learning algorithm but also on the URLLC load and interference footprint on the network.

APPENDIX A

DERIVING THE NUMBER OF ITERATIONS TO CONVERGE

The first-order necessary condition for local optimality is given by the vanishing of gradients. However, depending on the characteristics of the optimization landscape, equivalent conditions may be defined based on the objective functions. In the following subsections, we explore different optimization scenarios and provide examples of the bounds that can be leveraged to engineer K_{\min} . These alternative theoretical approaches complement the numerical design of K_{\min} , as illustrated in Equation (8).

Towards solving the distributed optimization problem (1), the central node performs the gradient descent update at the k th iteration as

$$\mathbf{w}_{k+1} = \mathbf{w}_k - \frac{\eta_k}{n} \sum_{i \in \mathcal{N}_{n,k}} \hat{\nabla} f_i(\mathbf{w}_k), \quad (\text{A.1})$$

where the right hand side of the equation represents $A(\cdot)$ in (2a), $\hat{\nabla} f_i(\mathbf{w}_k)$ is the true gradient's noisy estimation at

the i th AI device, and $\mathcal{N}_{n,k}$ is the set of AI devices from which central node received the first n local updates at the k th iteration. We assume that each AI device employs mini-batch gradient descent, and to simplify our notation, the size of the mini-batches is assumed to be the same for all devices in all iterations. For the sake of simplicity, we assume that the gradients' noise is independent and identically distributed [54]. Notice that the numerical approximations of K_{\min} do not rely on the gradient noise assumption, and we need this assumption only for the theoretical approximation of K_{\min} .

The overall gradient estimate using the local estimates of the AI devices can be obtained as

$$\frac{1}{n} \sum_{i \in \mathcal{N}_{n,k}} \widehat{\nabla} f_i(\mathbf{w}_k) := \nabla f(\mathbf{w}_k) + \bar{\mathbf{e}}_k^{(n)}, \quad (\text{A.2})$$

where $\bar{\mathbf{e}}_k^{(n)} := \frac{1}{n} \sum_{i \in \mathcal{N}_{n,k}} \mathbf{e}_{i,k}$, and $\mathbf{e}_{i,k}$ is the residual term of the i th device's estimate at the k th iteration, while $\nabla f(\mathbf{w}_k)$ is the true gradient (i.e., the gradient of the batch gradient descent on centralized training).

A. DGD, Strongly Convex Objective Functions

Assumption 1. [22], [55] The objective functions $f_i, \forall i \in \mathcal{N}$, are all L -smooth, with Lipschitz constant $L > 0$.

Assumption 2. [22], [55] The objective functions $f_i, \forall i \in \mathcal{N}$, are all strongly convex, with constant $\mu > 0$.

Assumption 3. [22] There exist $\beta_2 \geq (\beta_1 + 1)^2 > 0$ that, for $\forall k \in [K]$ and $\forall i \in \mathcal{N}$, the objective function $f(\mathbf{w})$ and the DGD algorithm have the following limits:

$$\nabla f(\mathbf{w}_k)^\top \mathbb{E}[\mathbf{e}_{i,k}] \geq \beta_1 \|\nabla f(\mathbf{w}_k)\|_2^2, \quad (\text{A.3a})$$

$$\nabla f(\mathbf{w}_k)^\top \mathbb{E}[\mathbf{e}_{i,k}] \leq \beta_2 \|\nabla f(\mathbf{w}_k)\|_2^2. \quad (\text{A.3b})$$

It is worth noting that (A.3a) implies that the noisy estimation of the gradient is on the same half space with the true gradient, and (A.3b) is a weaker assumption of the bounded variance of $\sum_{i \in \mathcal{N}_{n,k}} \widehat{\nabla} f_i(\mathbf{w}_k)/n$, and only bounds it by the actual gradient, $\nabla f(\mathbf{w}_k)$.

Assumption 4. [22], [55] The variance of the gradient norms in each device is bounded, i.e.,

$$\mathbb{E}[\|\mathbf{e}_{i,k}\|_2^2] \leq \sigma^2, \forall k \in [K], \forall i \in \mathcal{N}. \quad (\text{A.4})$$

Since, $\bar{\mathbf{e}}_k^{(n)}$ is an unbiased estimator of $\mathbb{E}[\mathbf{e}_{i,k}]$, we have

$$\mathbb{E}[\|\bar{\mathbf{e}}_k^{(n)}\|_2^2] \leq \frac{\sigma^2}{n}, \forall k \in [K]. \quad (\text{A.5})$$

Notably, from (A.3b) and (A.4), we can derive

$$\mathbb{E}[\|\widehat{\nabla} f_i(\mathbf{w}_k)\|_2^2] \leq \sigma^2 + \beta_2 \|\nabla f(\mathbf{w}_k)\|_2^2. \quad (\text{A.6})$$

Then, if Assumptions 1-4 hold, for a fixed learning rate η

that is $0 < \eta \leq \frac{\beta_1+1}{(2\beta_2+1)L}$, we have [22, Theorem 4.6]

$$\mathbb{E}[f(\mathbf{w}_k) - f(\mathbf{w}^*)] \leq \frac{\eta L \sigma^2}{2n\beta_1\mu} + (1 - \eta\beta_1\mu)^{k-1} \left(f(\mathbf{w}_1) - f(\mathbf{w}^*) - \frac{\eta L \sigma^2}{2n\beta_1\mu} \right), \quad (\text{A.7})$$

where the first term represents the gap to the expected optimal value that DGD converges to when $k \rightarrow \infty$ for a fixed learning rate, and the second term is the convergence rate. Using the learning rate bound and Assumption 3, and the fact that $\mu \leq L$ (as a result of Assumption 1 and 2), we can derive that $\eta\beta_1\mu < 1$, and hence, $(1 - \eta\beta_1\mu)$ is a contraction factor.

Let us assume that our initial point is within a bounded region with respect to the final point that we can converge (i.e., the last parenthesis in (A.7) is less than or equal to W^A). Note that the additional term of $\eta L \sigma^2 / 2n\beta_1\mu$ reflects that DGD cannot converge to the optimal value, but instead, to a neighborhood of $f(\mathbf{w}^*)$. Then, the minimum required number of iterations, K_{\min} , to reach ϵ -optimality becomes

$$K_{\min} \geq \log_{(1-\eta\beta_1\mu)} \left(\epsilon - \frac{\eta L \sigma^2}{2n\beta_1\mu} \right) - \log_{(1-\eta\beta_1\mu)}(W) + 1. \quad (\text{A.8})$$

Then, (A.8) can be simplified as

$$K_{\min} \geq \log_b \left(\frac{W^A}{\epsilon - \frac{z^A}{n}} \right) + 1, \quad (\text{A.9})$$

where $b := 1/(1 - \eta\beta_1\mu) > 1$, and z^A is a positive constant which depends on the learning rate, Lipschitz constant, strong convexity, and the error in the gradient estimates for $n=1$.

B. DGD, Non-convex Objective Functions

Assumption 5. [22] The objective functions $f_i, \forall i \in \mathcal{N}$, are lower bounded by a scalar f_{\inf} for all sequences of \mathbf{w}_k .

The non-convex objective functions may contain several local minima and other stationary points. Therefore, we define the convergence criteria on the gradient. Then, if Assumptions 1, 3-5 hold, for a fixed learning rate satisfying $0 < \eta \leq \frac{\beta_1+1}{L(2\beta_2+1)}$, we have [22, Theorem 4.8]

$$\mathbb{E} \left[\frac{1}{K} \sum_{k=1}^K \|\nabla f(\mathbf{w}_k)\|_2^2 \right] \leq \frac{\eta L \sigma^2}{n(\beta_1+1)} + \frac{2(f(\mathbf{w}_1) - f_{\inf})}{\eta(\beta_1+1)K}. \quad (\text{A.10})$$

To understand (A.10), consider centralized training and batch gradient descent, where there exist no gradient noise, and σ^2 becomes zero, resulting in $\|\nabla f(\mathbf{w}_k)\|_2 \rightarrow 0$ as K enlarges. However, in DGD, the average norm of gradients converges to $\eta L \sigma^2 / n(\beta_1+1)$. Now, the required number of iterations, K_{\min} , to reach ϵ -optimality becomes

$$K_{\min} \geq \frac{2(f(\mathbf{w}_1) - f_{\inf})}{\eta(\beta_1+1) \left(\epsilon - \frac{\eta L \sigma^2}{n(\beta_1+1)} \right)}. \quad (\text{A.11})$$

In (A.11), we observe that loosening the convergence criteria (i.e., as ϵ increases) reduces the required number of iterations

to reach ϵ -optimality gap. We can simplify (A.11) as

$$K_{\min} \geq \frac{W^B}{\epsilon - \frac{z^B}{n}}, \quad (\text{A.12})$$

where $W^B := 2(f(\mathbf{w}_1) - f_{\inf})/\eta(\beta_1 + 1)$, and z^B is a function of the learning rate, Lipschitz constant, and error in the gradient estimates when $n=1$. Note that ϵ should be set to a value larger than the neighborhood DGD can potentially converge to.

C. FL, Strongly Convex Objective Functions

There are two main differences between FL and DGD, i) there could be several local iterations in each AI device between two communications, and ii) the model parameters (i.e., the weights of the DNNs) are communicated, rather than the gradients in DGD. Hence, on the local update, each AI device performs (A.1) for E times before updating the global iteration k , as (2b).

Assumption 6. [55] The variance of the gradient estimates in each AI device is bounded, i.e.,

$$\mathbb{E} \left[\left\| \widehat{\nabla} f_i(\mathbf{w}_k) \right\|^2 \right] \leq G^2. \quad (\text{A.13})$$

Note that (A.13) is a stricter assumption than Assumptions 3 and 4, combined, as shown in (A.6).

If Assumptions 1, 2, 4, and 6 hold, and n AI devices are selected uniformly at each iteration, then for a diminishing learning rate $\eta_k = 2/(\mu(\xi + k + \kappa))$, where $\kappa \in [E-1]$ is the local iteration number and $\xi := \max\{8L/\mu, E\}$, the following inequality holds [55, Theorem 3]:

$$\mathbb{E}[f(\mathbf{w}_k) - f(\mathbf{w}^*)] \leq \frac{2L \left(\frac{\sigma^2}{N} + 8(E-1)^2 + \rho E^2 G^2 + \xi G^2 \right)}{\mu^2(\xi + k + \kappa - 1)}, \quad (\text{A.14})$$

where $\rho := \frac{4(N-n)}{n(N-1)}$. Hence, the minimum number of global iterations (i.e., rounds of communications) to attain ϵ -optimality approximately becomes [55]

$$K_{\min} \propto \frac{1}{\epsilon} \left[\left(1 + \frac{1}{n} \right) E G^2 + \frac{\frac{\sigma^2}{N} + G^2}{E} + G^2 \right], \quad (\text{A.15})$$

where we assumed $\xi = O(1 + E)$.

APPENDIX B BASE 3GPP CHANNEL MODEL

To model the channel, we consider a multiple-input and multiple-output system in which we leverage the time-varying 3D spatial channel model from 3GPP in [39]. In this model, channels are characterized via clustering the multipath components, arriving at antenna arrays, in delay and double-directional angle (i.e., the zenith and azimuth of the angle-of-arrivals at the receiver and angle-of-departures at the transmitter). For simplicity, let us assume that N_g and N_d are respectively the number of antenna elements of gNB and devices. We denote by $\mathbf{H}_{x,y}(\tau; t) \in \mathbb{C}^{N_d \times N_g}$ the baseband channel response at time t to an input impulse at time $t - \tau$, between the x th device and y th gNB in DL. Then, an entry

of $\mathbf{H}_{x,y}(\tau; t)$ for the p th receiving antenna element and q th transmitting antenna element can be computed as

$$[\mathbf{H}_{x,y}(\tau; t)]_{p,q} := \sqrt{\beta^{x,y}} \sum_{l=1}^{N_c} \sqrt{P_l^{x,y}} \sum_{s=1}^{N_s} (\mathbf{g}_p^{x,y}(t, l, s))^T \mathbf{F}_{xp}^{x,y}(t, l, s) \mathbf{g}_q^{x,y}(t, l, s) e^{jY_{p,q}^{x,y}(t, l, s)} \delta(\tau - \tau_{p,l,s}), \quad (\text{A.16})$$

where N_c and N_s are, respectively, the number of clusters and rays. $\beta^{x,y}$ accounts for path loss and shadowing, which vary depending on the scenario (e.g., urban, indoor, etc.), and $P_l^{x,y}$ is a function of l th cluster normalized power. In Appendix C, we have specified details of $\beta^{x,y}$ for our InF-DH scenario. Besides, $\mathbf{g}_p^{x,y}(\cdot)$ is the field patterns of the p th receiving element that the s th ray of the l th cluster has in the direction defined by the arriving zenith and azimuth angles, $\mathbf{F}_{xp}^{x,y}(\cdot)$ is a 2×2 matrix modeling the cross polarization power ratio for the s th ray of the l th cluster, $\mathbf{g}_q^{x,y}(\cdot)$ is the field patterns of the q th transmitting element that the s th ray of the l th cluster has in the direction defined by the departing zenith and azimuth angles, $Y_{p,q}^{x,y}(\cdot)$ is a function of the location vector of the p th receiving and q th transmitting element as well as the Doppler frequency, and finally, $\tau_{p,l,s}$ is the propagation delay of the s th ray in the l th cluster. For UL, $\mathbf{H}_{x,y}(\tau; t)$ can be derived by swapping p and q in (A.16).

APPENDIX C

INF-DH SCENARIO OF THE BASE 3GPP CHANNEL MODEL

In this appendix, we specify the parameters of the base 3GPP channel model based on InF-DH scenario [39], used in our simulations. The clutter in InF-DH scenario typically represent small to medium-sized metallic machines and irregularly shaped objects. To calculate $\beta_l^{x,y}$ in (A.16), the path loss is calculated by tracing the degradation in signal strength over distance under line-of-sight (LOS) and non-LOS (NLOS) circumstances. The path loss under LOS and NLOS assumptions are given by [39]

$$PL_{\text{LOS}}(d_{x,y}^{3D})[\text{dB}] = 31.84 + 21.5 \log_{10}(d_{x,y}^{3D}) + 19 \log_{10}(f_c), \quad (\text{A.17a})$$

$$PL_{\text{NLOS}}(d_{x,y}^{3D})[\text{dB}] = \max(PL_{\text{LOS}}(d_{x,y}^{3D}), PL_{\text{DH}}(d_{x,y}^{3D})), \quad (\text{A.17b})$$

where

$$PL_{\text{DH}}(d_{x,y}^{3D})[\text{dB}] = 33.63 + 21.9 \log_{10}(d_{x,y}^{3D}) + 20 \log_{10}(f_c). \quad (\text{A.18})$$

In above equations, d_{3D} and f_c denote the 3D distance between the device and gNB, and the center frequency, respectively. In InF-DH, the LOS probability is described by [39]

$$\text{Pr}_{\text{LOS}}(d_{x,y}^{2D}) = \exp \left(\frac{d_{x,y}^{2D} \ln(1 - r_{\text{clut}}) (h_{\text{clut}} - h_{\text{device}})}{d_{\text{clut}} (h_{\text{gNB}} - h_{\text{device}})} \right), \quad (\text{A.19})$$

where d_{2D} represents the ground distance between gNB and the device. Besides, h_{gNB} , h_{device} , d_{clut} , h_{clut} , and r_{clut} denote the gNB's antenna height, devices' antenna height, the typical clutter size, height and density, and are set in our simulations to 8 m, 1.5 m, 2 m, 6 m, and 60%, respectively. The shadowing

for LOS and NLOS is assumed to follow a zero-mean log-normal distribution with standard deviation 4.3 and 4 in dB, respectively. In our link level simulations, we first set the position of the 4 gNBs, as shown in Fig. 2. Then, for each pair of possible device positions and the 4 gNB positions, we generate uncorrelated link conditions with $\text{Pr}_{\text{LOS}}(d_{2D})$ for LOS, and $1 - \text{Pr}_{\text{LOS}}(d_{2D})$ for NLOS. Assuming that Ω_{LOS} and Ω_{NLOS} are random variables denoting the shadowing for LOS and NLOS, respectively, then we have

$$\beta^{x,y} := \begin{cases} 10^{\frac{-\text{Pr}_{\text{LOS}}(d_{x,y}^{3D}) - \Omega_{\text{LOS}}}{10}}, & \text{with probability } \text{Pr}_{\text{LOS}}, \\ 10^{\frac{-\text{Pr}_{\text{NLOS}}(d_{x,y}^{3D}) - \Omega_{\text{NLOS}}}{10}}, & \text{with probability } 1 - \text{Pr}_{\text{LOS}}. \end{cases} \quad (\text{A.20})$$

Nevertheless, the large-scale parameters are generated with a correlation distance of 10 m in the horizontal plane. Then, we followed the spatial consistency procedure in [39, §7.5, §7.6.3] to generate small-scale parameters and channel coefficients and used the parameters in [39, Table 7.5-6 Part-3].

REFERENCES

- [1] H. Xu, J. Wu, Q. Pan, X. Guan, and M. Guizani, "A survey on digital twin for industrial internet of things: Applications, technologies and tools," *IEEE Commun. Surveys Tuts.*, vol. 25, no. 4, pp. 2569–2598, 2023.
- [2] D. Gündüz, D. B. Kurka, M. Jankowski, M. M. Amiri, E. Ozfatura, and S. Sreekumar, "Communicate to learn at the edge," *IEEE Commun. Mag.*, vol. 58, no. 12, pp. 14–19, 2020.
- [3] A. Alabbasi, M. Ganjalizadeh, K. Vandikas, and M. Petrova, "On cascaded federated learning for multi-tier predictive models," in *IEEE Int. Conf. Commun. Workshops (ICC Workshops)*, 2021.
- [4] H. Huang *et al.*, "Real-time fault detection for IIoT facilities using GBRBM-based DNN," *IEEE Internet Things J.*, vol. 7, no. 7, pp. 5713–5722, 2020.
- [5] A. Hammoud, H. Otrouk, A. Mourad, and Z. Dziong, "On demand fog federations for horizontal federated learning in IoV," *IEEE Trans. Netw. Service Manag.*, vol. 19, no. 3, pp. 3062–3075, 2022.
- [6] B. McMahan, E. Moore, D. Ramage, S. Hampson, and B. A. y. Arcas, "Communication-efficient learning of deep networks from decentralized data," in *Proc. Int. Conf. Artif. Intell. Stat. (AISTATS)*, 2017.
- [7] S. Dutta, G. Joshi, S. Ghosh, P. Dube, and P. Nagpurkar, "Slow and stale gradients can win the race: Error-runtime trade-offs in distributed SGD," in *Proc. Int. Conf. Artif. Intell. Stat. (AISTATS)*, 2018.
- [8] X. Yu, Y. Lin, Z. Gao, H. Du, and D. Niyato, "Dynamic and fast convergence for federated learning via optimized hyperparameters," *IEEE Trans. Netw. Service Manag.*, early access, 2024.
- [9] M. Chen *et al.*, "Distributed learning in wireless networks: Recent progress and future challenges," *IEEE J. Sel. Areas Commun.*, vol. 39, no. 12, pp. 3579–3605, 2021.
- [10] *Service requirements for cyber-physical control applications in vertical domains*, 3GPP, TS 22.104 v19.2.0, 2024.
- [11] *Service requirements for the 5G system*, 3GPP, TS 22.261 v20.1.0, 2025.
- [12] O. L. A. López *et al.*, "Statistical tools and methodologies for ultra-reliable low-latency communication—a tutorial," *Proc. IEEE*, vol. 111, no. 11, pp. 1502–1543, 2023.
- [13] "AI-RAN alliance vision and mission," AI-RAN Alliance, White Paper, 2024.
- [14] A. K. Bairagi *et al.*, "Coexistence mechanism between eMBB and uRLLC in 5G wireless networks," *IEEE Trans. Commun.*, vol. 69, no. 3, pp. 1736–1749, 2021.
- [15] U. Bucci, D. Cassioli, and A. Marotta, "Performance of spatially diverse URLLC and eMBB traffic in cell free massive MIMO environments," *IEEE Trans. Netw. Service Manag.*, vol. 21, no. 1, pp. 161–173, 2024.
- [16] M. Alsenwi, E. Lagunas, and S. Chatzinotas, "Distributed learning framework for eMBB-URLLC multiplexing in open radio access networks," *IEEE Trans. Netw. Service Manag.*, vol. 21, no. 5, pp. 5718–5732, 2024.
- [17] L. Valentini, E. Bernardi, F. Saggese, M. Chiani, E. Paolini, and P. Popovski, "Contention-based mMTC/URLLC coexistence through coded random access and massive MIMO," *IEEE J. Sel. Topics Signal Process.*, early access, 2024.
- [18] P. Popovski, K. F. Trillingsgaard, O. Simeone, and G. Durisi, "5G wireless network slicing for eMBB, URLLC, and mMTC: A communication-theoretic view," *IEEE Access*, vol. 6, pp. 55 765–55 779, 2018.
- [19] M. Ganjalizadeh, H. S. Ghadikolaei, J. Haraldson, and M. Petrova, "Interplay between distributed AI workflow and URLLC," in *IEEE Global Commun. Conf. (GLOBECOM)*, 2022.
- [20] *5G System (5GS); Study on traffic characteristics and performance requirements for AI/ML model transfer*, 3GPP, TR 22.874 v18.2.0, 2021.
- [21] *Study on AI/ML Model Transfer Phase2*, 3GPP, TR 22.876 v19.1.0, 2023.
- [22] L. Bottou, F. Curtis, and J. Nocedal, "Optimization methods for large-scale machine learning," *SIAM Review*, vol. 60, no. 2, pp. 223–311, 2018.
- [23] K. Scaman, F. Bach, S. Bubeck, L. Massoulié, and Y. T. Lee, "Optimal algorithms for non-smooth distributed optimization in networks," *Adv. Neural Inf. Process. Syst. (NeurIPS)*, vol. 31, 2018.
- [24] T. Li, A. K. Sahu, A. Talwalkar, and V. Smith, "Federated learning: Challenges, methods, and future directions," *IEEE Signal Process. Mag.*, vol. 37, no. 3, pp. 50–60, 2020.
- [25] H. S. Ghadikolaei, S. Stich, and M. Jaggi, "LENA: Communication-efficient distributed learning with self-triggered gradient uploads," in *Proc. Int. Conf. Artif. Intell. Stat. (AISTATS)*, 2021.
- [26] S. Ji, W. Jiang, A. Walid, and X. Li, "Dynamic sampling and selective masking for communication-efficient federated learning," *IEEE Intell. Syst.*, vol. 37, no. 2, pp. 27–34, 2022.
- [27] T. Chen, G. Giannakis, T. Sun, and W. Yin, "LAG: Lazily aggregated gradient for communication-efficient distributed learning," in *Adv. Neural Inf. Process. Syst. (NeurIPS)*, 2018.
- [28] M. Chen, Z. Yang, W. Saad, C. Yin, H. V. Poor, and S. Cui, "A joint learning and communications framework for federated learning over wireless networks," *IEEE Trans. Wireless Commun.*, vol. 20, no. 1, pp. 269–283, 2021.
- [29] C. T. Dinh *et al.*, "Federated learning over wireless networks: Convergence analysis and resource allocation," *IEEE/ACM Trans. Netw.*, vol. 29, no. 1, pp. 398–409, 2021.
- [30] W. Hou *et al.*, "Adaptive training and aggregation for federated learning in multi-tier computing networks," *IEEE Trans. Mobile Comput.*, vol. 23, no. 5, pp. 4376–4388, 2024.
- [31] W. Xia, T. Q. S. Quek, K. Guo, W. Wen, H. H. Yang, and H. Zhu, "Multi-armed bandit-based client scheduling for federated learning," *IEEE Trans. Wireless Commun.*, vol. 19, no. 11, pp. 7108–7123, 2020.
- [32] P. Zhang, C. Wang, C. Jiang, and Z. Han, "Deep reinforcement learning assisted federated learning algorithm for data management of IIoT," *IEEE Trans. Ind. Informat.*, vol. 17, no. 12, pp. 8475–8484, 2021.
- [33] W. Zhang *et al.*, "Optimizing federated learning in distributed industrial IIoT: A multi-agent approach," *IEEE J. Sel. Areas Commun.*, vol. 39, no. 12, pp. 3688–3703, 2021.
- [34] M. M. Amiri, D. Gündüz, S. R. Kulkarni, and H. V. Poor, "Convergence of update aware device scheduling for federated learning at the wireless edge," *IEEE Trans. Wireless Commun.*, vol. 20, no. 6, pp. 3643–3658, 2021.
- [35] M. E. Ozfatura, J. Zhao, and D. Gündüz, "Fast federated edge learning with overlapped communication and computation and channel-aware fair client scheduling," in *IEEE Int. Workshop Signal Process. Adv. Wireless Commun. (SPAWC)*, 2021.
- [36] M. M. Amiri, D. Gündüz, S. R. Kulkarni, and H. V. Poor, "Convergence of federated learning over a noisy downlink," *IEEE Trans. Wireless Commun.*, vol. 21, no. 3, pp. 1422–1437, 2022.
- [37] A. M. Albaser, M. Abdallah, A. Al-Fuqaha, A. M. Seid, A. Erbad, and O. A. Dobre, "Fair selection of edge nodes to participate in clustered federated multitask learning," *IEEE Trans. Netw. Service Manag.*, vol. 20, no. 2, pp. 1502–1516, 2023.
- [38] E. Dahlman, S. Parkvall, and J. Skold, *5G NR: The next generation wireless access technology*, 2nd ed. New York, NY, USA: Academic, 2020.
- [39] *Study on channel model for frequencies from 0.5 to 100 GHz*, 3GPP, TR 38.901 v18.0.0, 2024.
- [40] "Service-level specifications (SLSs) for 5G technology-enabled connected industries," 5G Alliance for Connected Industries and Automation (5G-ACIA), Frankfurt, Germany, White Paper, 2021.
- [41] M. Ganjalizadeh, A. Alabbasi, J. Sachs, and M. Petrova, "Translating cyber-physical control application requirements to network level parameters," in *IEEE Int. Symp. Pers., Indoor, Mobile Radio Commun. (PIMRC)*, 2020.
- [42] M. Ganjalizadeh, H. S. Ghadikolaei, A. Azari, A. Alabbasi, and M. Petrova, "Saving energy and spectrum in enabling URLLC services:

- A scalable RL solution,” *IEEE Trans. Ind. Informat.*, vol. 19, no. 10, pp. 10 265–10 276, Oct. 2023.
- [43] P. Popovski *et al.*, “Wireless access in ultra-reliable low-latency communication (URLLC),” *IEEE Trans. Commun.*, vol. 67, no. 8, pp. 5783–5801, 2019.
 - [44] T. Tatarenko and B. Touri, “Non-convex distributed optimization,” *IEEE Trans. Autom. Control*, vol. 62, no. 8, pp. 3744–3757, 2017.
 - [45] T. Haarnoja *et al.*, “Soft actor-critic algorithms and applications,” 2018, *arXiv:1812.05905* [cs.LG].
 - [46] M. Bennis, M. Debbah, and H. V. Poor, “Ultrareliable and low-latency wireless communication: Tail, risk, and scale,” *Proc. IEEE*, vol. 106, no. 10, pp. 1834–1853, Oct. 2018.
 - [47] C. Tessler, D. J. Mankowitz, and S. Mannor, “Reward constrained policy optimization,” in *Int. Conf. Learn. Represent. (ICLR)*, 2019.
 - [48] P. L. Donti, D. Rolnick, and J. Z. Kolter, “DC3: A learning method for optimization with hard constraints,” in *Int. Conf. Learn. Represent. (ICLR)*, 2021.
 - [49] S. Fujimoto, H. van Hoof, and D. Meger, “Addressing function approximation error in actor-critic methods,” in *Proc. Int. Conf. Mach. Learn. (ICML)*, 2018.
 - [50] A. G. Howard *et al.*, “MobileNets: Efficient convolutional neural networks for mobile vision applications,” 2017, *arXiv:1704.04861* [cs.CV].
 - [51] S. Magnusson, H. S. Ghadikolaei, and N. Li, “On maintaining linear convergence of distributed learning and optimization under limited communication,” *IEEE Trans. Signal Process.*, vol. 68, pp. 6101–6116, 2020.
 - [52] T. Schaul, J. Quan, I. Antonoglou, and D. Silver, “Prioritized experience replay,” in *Int. Conf. Learn. Represent. (ICLR)*, 2016.
 - [53] E. L. Kaplan and P. Meier, “Nonparametric estimation from incomplete observations,” *J. Amer. Statistical Assoc.*, vol. 53, no. 282, pp. 457–481, 1958.
 - [54] M. Cohen, J. Diakonikolas, and L. Orecchia, “On acceleration with noise-corrupted gradients,” in *Proc. Int. Conf. Mach. Learn. (ICML)*, 2018.
 - [55] X. Li, K. Huang, W. Yang, S. Wang, and Z. Zhang, “On the convergence of FedAvg on non-IID data,” in *Int. Conf. Learn. Represent. (ICLR)*, 2020.